6-2017

Anatomical and Behavioral Investigation of C1ql3 in the Mouse Suprachiasmatic Nucleus

David C. Martinelli
University of Connecticut School of Medicine and Dentistry

HHS Public Access

Author manuscript

J Biol Rhythms. Author manuscript; available in PMC 2017 November 01.

Published in final edited form as:

J Biol Rhythms. 2017 June ; 32(3): 222–236. doi:10.1177/0748730417704766.

Anatomical and Behavioral Investigation of *C1ql3* in the Mouse Suprachiasmatic Nucleus

Kylie S. Chew[*,†], **Diego C. Fernandez**[*,1], **Samer Hattar**[*,‡,1], **Thomas C. Südhof**[§,‖], and **David C. Martinelli**[§,¶,2]

[*]Department of Biology, The Johns Hopkins University, Baltimore, Maryland [†]Department of Biology, Stanford University School of Medicine, Stanford, California [‡]The Solomon Snyder-Department of Neuroscience, Johns Hopkins University School of Medicine, Baltimore, Maryland [§]Department of Molecular and Cellular Physiology, Stanford University School of Medicine, Stanford, California [‖]Howard Hughes Medical, Institute, Stanford University School of Medicine, Stanford, California [¶]Department of Neuroscience, University of Connecticut Health Center, Farmington, Connecticut

Abstract

Many biochemical, physiological, and behavioral processes such as glucose metabolism, body temperature, and sleep-wake cycles show regular daily rhythms. These circadian rhythms are adjusted to the environmental light-dark cycle by a central pacemaker located in the suprachiasmatic nucleus (SCN) in order for the processes to occur at appropriate times of day. Here, we investigated the expression and function of a synaptic organizing protein, C1QL3, in the SCN. We found that *C1ql3* is robustly expressed in the SCN. *C1ql3* knockout mice have a reduced density of excitatory synapses in the SCN. In addition, these mice exhibited less consolidated activity to the active portions of the day and period lengthening following a 15-minute phase-delaying light pulse. These data identify C1QL3 as a signaling molecule that is highly expressed in SCN neurons, where it contributes to the formation and/or maintenance of glutamatergic synapses and plays a role in circadian behaviors, which may include circadian aftereffects.

Keywords

rhythms; circadian; aftereffects; suprachiasmatic nucleus; synapse; SCN; C1ql; C1q-like; C1ql3

Due to the rotation of the earth, organisms experience a 24-hour light-dark (LD) cycle. Daily rhythms of biochemical, physiological, and behavioral processes have been widely observed

[2]To whom all correspondence should be addressed: David C. Martinelli, Neuroscience Department, UConn Health Center, Room L4003, 263 Farmington Avenue, Farmington, CT 06030; martinelli.uchc@gmail.com.

[1]Present address: Section on Light and Circadian Rhythms (SLCR), National Institute of Mental Health, National Institute of Health, Bethesda, MD 20892.

CONFLICT OF INTEREST STATEMENT

The author(s) have no potential conflicts of interest with respect to the research, authorship, and/or publication of this article.

NOTE

Supplementary material is available for this article online.

in plants, animals, fungi, and cyanobacteria (Refinetti, 2005). Such daily rhythms are termed *circadian* rhythms from the Latin words *circa*, meaning "around," and *diem*, meaning "day." Environmental stimuli such as LD cycles, food availability, social cues, and temperature that entrain circadian clocks are called *zeitgebers* (German for "time givers"). The most powerful environmental entrainer is the solar day. Establishing an appropriate phase angle between circadian rhythms and the LD cycle is the foremost function of the circadian system because it ensures that biochemical, physiological, and behavioral processes occur at appropriate times.

Under constant dark (DD) conditions, circadian free-running periods are usually highly precise from day to day, yet they can be modulated by prior environmental conditions, a phenomenon referred to as *aftereffects*. For example, entraining mice to short or long days (20 or 28 hours) results in a shortened or lengthened circadian period, respectively, that persists in DD for months (Aschoff, 1960; Pittendrigh, 1960; Pittendrigh and Daan, 1976). Ambient temperature, light intensity (in constant light), developmental stage, and prior history can also produce aftereffects on the circadian period length (Aschoff, 1960, 1981; Barrett and Page, 1989; Eskin, 1971). Because the free-running period affects phase angles, aftereffects are likely very important for entrainment of circadian rhythms under natural conditions, especially regarding seasonal tracking. However, the mechanisms underlying aftereffects are poorly understood (Johnson et al., 2003).

Circadian rhythms are generated by an oscillatory transcriptional-translational feedback loop. In mammals, such clocks have been detected in many organs and cell types (Balsalobre et al., 1998; Dibner et al., 2010; Mohawk et al., 2012; Nagoshi et al., 2004; O'Neill and Reddy, 2011; Welsh et al., 2004; Yoo et al., 2004). These peripheral clocks are synchronized to each other and with the environmental LD cycle by the master circadian pacemaker, which is housed in the suprachiasmatic nucleus (SCN) and receives light information directly from the retina. While the mechanism for aftereffects assuredly affects the SCN, there is evidence for extra-SCN influences on aftereffects (Aton et al., 2004; Matsumoto et al., 1996; Molyneux et al., 2008). Specifically, replacing the SCN of an animal that was exhibiting aftereffects with an SCN from an unaffected donor did not abolish aftereffects (Matsumoto et al., 1996). Furthermore, the eye is not required for aftereffects to be sustained (Aton et al., 2004), and there is a strong negative correlation between the behavioral circadian period of mice exhibiting aftereffects and the SCN period of those mice measured in vitro (Molyneux et al., 2008). Finally, from studies in humans it has been proposed that neural plasticity may underlie aftereffects (Meijer et al., 2010; Scheer et al., 2007).

Neural plasticity is a broad term encompassing any changes in the number and/or strength of synaptic connections. These changes occur through synaptogenesis, synaptic pruning, or Hebbian or homeostatic synaptic plasticity. Hundreds of proteins have been implicated in regulating neural plasticity. One example is the secreted and presynaptically targeted protein complement component 1, q subcomponent-like 3 (C1QL3). *C1ql3* is expressed almost exclusively in a subset of excitatory neurons in the brain, mostly in the telencephalon, and promotes excitatory synaptogenesis and synapse maintenance (Iijima et al., 2010; Martinelli et al., 2016). C1QL3 is a high-affinity ligand for the postsynaptically localized BAI3 adhesion G protein-coupled receptor (GPCR; renamed ADGRB3; Hamann et al., 2015),

suggesting a possible transsynaptic signaling pathway for regulating synapse density (Bolliger et al., 2011). Additionally, C1QL3 was recently shown to transsynaptically regulate recruitment of kainate receptors to the postsynapse independently of BAI3 in the hippocampus (Matsuda et al., 2016). During our previous examinations of *C1ql3* (Martinelli et al., 2016), we noted *C1ql3* expression in the SCN. Thus, for this study we aimed to characterize its expression and investigate its function in this brain region.

Here we demonstrate that *C1ql3* is robustly expressed in a subset of SCN neurons and unexpectedly that *C1ql3* knockout (KO) mice have reduced excitatory synapse density in the SCN. We then investigated whether these changes in the structure of synaptic circuits in the SCN correlate with altered circadian behavior. We found that *C1ql3* KO mice exhibited increased wheel-running activity during the light portions of the circadian cycle (i.e., less consolidated activity to the night portion of a standard light-dark housing cycle) and period lengthening following a 15-minute phase-delaying light pulse suggestive of enhanced aftereffects. These results indicate that C1QL3 is a key signaling molecule in the formation and/or maintenance of synaptic circuits in the SCN and is important for regulation of multiple circadian behaviors.

METHODS

Mice

The analysis of *C1ql3* expression was performed using the IRES-mVenus knock-in allele (*C1ql3*^{flox}; C1ql3$^{tm1.1Sud}$ RRID: MGI_5779515) described by Martinelli et al. (2016). Behavior experiments were performed on littermate male mice. The *C1ql3*^{flox} allele was converted to the null allele *(C1ql3*$^{-}$*)* by crossing to B6.C-Tg(CMV-cre)1Cgn/J mice. *C1ql3*$^{+/+}$ and *C1ql3*$^{-/-}$ (C1ql3$^{tm1.2Sud}$ RRID: MGI_5779517) mice were obtained by breeding *C1ql3*$^{+/-}$ mice. The background strain of the mice was C57BL/6.

Immunofluorescence

Animals were prepared for immunofluorescence studies by transcardial perfusion with 4% PFA, followed by dissection of the brain and cryoprotection in 30% sucrose for 2 days. Brains were cryosectioned at 20-μM sections onto glass slides. In preparation for immunofluorescence, tissue was blocked with 5% goat serum and 0.3% Triton X-100 diluted into phosphate-buffered saline (PBS) for 1 hour at room temperature, and then primary antibodies diluted in blocking buffer were applied overnight at 4 °C. The following primary antibodies were used in this study on cryosections: rabbit anti-VIP (1:500; 20077 ImmunoStar, Hudson, Wisconsin), rabbit anti-AVP (1:500; 20069 ImmunoStar), rabbit anti-GRP (1:500; 20073 ImmunoStar), guinea pig anti-VGluT2 (1:1000; AB2251 Millipore, Hayward, California), rabbit anti-VGAT (1:1000; 131 003 Synaptic Systems, Goettingen, Germany), and mouse anti-SYP (1:1000; 7H12 Cell Signaling, Danvers, Massachusetts). The signal intensity of mVenus from the *C1ql3*^{flox} allele was low, so an anti-GFP antibody was used to enhance signal: rabbit anti-GFP (1:1000; A11122 Invitrogen, Carlsbad, California). Secondary Alexa Fluor antibodies (Life Technologies, Carlsbad, California) were used with appropriate fluorescent conjugates. After washing with PBS, secondary antibodies diluted in blocking buffer were applied for 1 hour at room temperature. After

washing, sections were mounted with a cover-slip and Fluoromount-G with DAPI mounting media (SouthernBiotech, Birmingham, Alabama).

Co-staining for mVenus (as a proxy for *C1ql3* expression) and either Brn3a or melanopsin in mouse retinas was performed as follows: Retinas were isolated from approximately 2-month-old $C1ql3^{flox/flox}$ mice. Isolated retinas were fixed for 1 hour in 4% paraformaldehyde in PBS. Retinas were then washed for 1 hour and placed in blocking solution of 0.3% Triton X-100 in PBS plus 3% BSA for 3 hours at room temperature. Retinas were then placed in blocking solution containing chicken anti-GFP (1:500; ab13970 Abcam, Cambridge, UK) and rabbit anti-Brn3a (1:250; AB5945 Millipore) and incubated at 4 °C overnight. Retinas were then washed 3 × 10 minutes in PBS before being placed in a secondary antibody solution containing blocking solution with a goat anti-chicken antibody conjugated to AF-488 (1:500; Invitrogen) and goat anti-rabbit AF-594 (1:500; Invitrogen). Retinas were then washed 3 × 10 minutes in PBS and mounted in Prolong Gold with DAPI (P36931 Thermofisher, Waltham, Massachusetts). Co-staining for mVenus and melanopsin was performed essentially as described above, but using rabbit anti-melanopsin antibody (1:500; AB-N38 Advanced Targeting Systems, San Diego, California) and incubated for 3 to 4 days at 4°C in the primary antibody solution.

For quantification of synaptic puncta density in Figure 3, images were acquired with a Nikon confocal microscope. Z-stacks, 10 μM thick, containing 10 confocal planes were collapsed into a single image. As first described by Martinelli et al. (2016), a novel program was coded for Mathmatica (Wolfram, Champaign, Illinois) to quantify synaptic puncta density. For each mouse, the SCN puncta densities of at least 3 cryosections centering around the middle of the SCN along its anteroposterior axis were averaged. This number was averaged with the means of other mice of the same genotype to create the final mean. The number of mice analyzed per genotype is displayed on each bar of the figure. Statistical tests are described in the figure legends.

Wheel-running Behavior

General set-up—All mouse work was approved by animal use committees at Stanford and Johns Hopkins Universities.

All mice were approximately 4 to 5 months old at the beginning of the recordings, and recordings continued for no more than 3 months. Exact sample sizes are listed in the figure legends, and individual data points are plotted on the figures themselves. Mice were housed individually with ad libitum food and water, and cages were changed at least every 2 weeks. All light bulbs used were Philips (Foster City, California) Daylight deluxe fluorescent lamps. For wheel-running activity, mice were provided with a 4.5-inch running wheel. General activity was measured using infrared motion detectors from Mini Mitter (Respironics, Murrysville, Pennsylvania) with the motion detector mounted to the top of the cage. All data were collected in 10-minute bins using Vitalview software (Mini Mitter, Respironics). Clocklab (Actimetrics, Wilmette, Illinois) was used to generate actograms and chi-square periodograms.

The following light paradigms were used: When general activity was measured by infrared beam breaks, WT and *C1ql3* KO mice were placed in a 12-hour/12 hour LD (12/12 LD) cycle (light portion 500 lux) for 2 weeks to assess photoentrainment. The mice were then place in DD for 1 week to assess free-running period. After this, phase shifting pulses were given at CT 15 (~750–1000 lux for 15 minutes), and the mice remained in DD for another week to assess any changes in free-running period caused by the phase shift. After DD, mice were exposed to a jet lag paradigm that included decreasing light intensities during the light portion of the cycle. For the first week after DD, mice were returned to a 12/12 LD cycle with the light portion at 500 lux. Then the light intensity was increased to 1000 lux for another 7 days. Next, a 6-hour delay was introduced to the LD cycle, and mice were allowed to reentrain for 7 days. Then another 6-hour delay was introduced to the LD cycle, and simultaneously the light intensity in light portion was decreased to 50 lux.

When wheel-running behavior was recorded, 2 different light paradigms were used: First (Fig. 5 and Suppl. Fig. SI 1) mice were placed under 12/12 LD (light portion 500 lux) for 4 weeks and then released into DD for 3 weeks. Then phase-shifting pulses were given at CT 15 (~750–1000 lux for 15 minutes), and the mice remained in DD for another week to assess any changes in free-running period caused by the phase shift. After DD, mice were placed in constant light (LL) for at least 2 weeks (500 lux). The second light cycle paradigm (Suppl. Fig. SI 2) was 2 weeks of 12/12 LD (light portion 500 lux) followed by 2 weeks of LL (500 lux).

Quantification—The total numbers of wheel revolutions in the light and dark portions of the 12/12 LD cycles were determined by summing the raw recorded data during the light and dark portions of the cycle. Results are plotted in Figure 5B and 5C. A 2-tailed *t* test was used to compare the values from WT and *C1ql3* KO mice.

Phase angles were calculated by using ClockLab (Actimetrics) to determine the onset of activity while mice were housed in 12/12 LD, and then the difference between the offset of light and the onset of activity was calculated for each day in 12/12 LD. The first 2 days in LD were excluded. The average for each animal is plotted in Figure 5D for wheel-running activity and Supplementary Figure SI 4B for general activity measured by infrared beam breaks. A 2-tailed *t* test was used to compare the values from WT and *C1ql3* KO mice in each case.

The stability of entrainment was determined by calculating the standard deviation of the onsets of activity under 12/12 LD. Mean standard deviations for each animal are plotted in Figure 5E (wheel running) and Supplementary Figure SI 4A (beam breaks). A 2-tailed *t* test was used to compare the values from WT and *C1ql3* KO mice in each case.

Chi-square periodograms were generated with ClockLab (Actimetrics) for LD, DD, and LL portions of all the recordings (Fig. 5A and Suppl. Figs. SI 1–3). In DD and LL, free-running periods were also calculated based on the slope of the onsets with ClockLab (Actimetrics) from 5 to 14 consecutive days of recording, based on the length of the recording. The first 2 days in constant darkness were excluded. A 2-way ANOVA with Bonferroni's multiple comparisons test was used to compare the free-running periods of WT and *C1ql3* KO mice

under DD conditions before and after a 15-minute light pulse at CT 15 (Fig. 5G). A 2-tailed *t* test was used to compare the change (delta) in period length of WT and *C1ql3* KO mice before and after the light pulse (Fig. 5H). A 2-tailed *t* test was also used to compare the period lengths of WT and *C1ql3* KO mice under LL conditions (Fig. 5I).

Phase shifting was quantified as follows: A predicted onset of activity was calculated by making a regression line based the onsets of activity under DD for 6 days prior to the 15-minute light pulse and extrapolating the predicted onset for the day following the light pulse. Then difference between this predicted onset and the actual onset following the light pulse was calculated and plotted in Figure 5F. A 2-tailed *t* test was used to compare the values from WT and *C1ql3* KO mice. Phase shifts are traditionally calculated as the difference between a regression line of the onsets of activity for at least 6 days before the light pulse and a regression line of the onsets of activity for at least 6 days after the light pulse (Albrecht and Oster, 2001; Aschoff, 1965; Jud et al., 2005). We could not follow this method of calculating the magnitude of phase shift in our experiments because in *C1ql3* KO mice the period length also changed dramatically following the light pulse.

During the jet lag paradigm, days to reentrainment were determined by measuring the onsets and offsets of activity using ClockLab (Actimetrics). Mice were defined as entrained once both the onset and offsets were consistent for at least 2 days. On and offsets were considered consistent if they varied by less than the standard deviation measured during the initial beam break recordings under 12/12 LD conditions. Results are plotted in Supplementary Figure SI 4C. A one-way ANOVA with Bonferroni's multiple comparisons test was used to compare days to reentrainment of WT and *C1ql3* KO mice for each of the 3 LD cycles following DD.

Masking during the jet lag paradigm was measured by summing the total number of beam breaks that occurred in the last 6 hours of the light portion of the cycle during the first 3 days following a 6-hour advance of the LD cycle (see orange box in Suppl. Fig. SI 3). Through masking mechanisms, light suppresses activity during this time while the mice were reentraining to the new LD cycle. Results are plotted in Supplementary Figure SI 4D. A 2-way ANOVA with Bonferroni's multiple comparisons test was used to compare masking of WT and *C1ql3* KO mice for each of the first 3 days following each of the two 6-hour advances in the LD cycle.

Criteria for exclusion—Several mice had either very low levels of activity or unstable rhythms, sometimes in general and sometimes only under LL conditions. This is apparent from both the actograms and periodograms from these animals. For wheel-running recordings, 1 *C1ql3* KO animal was arrhythmic in general (first actogram and corresponding periodograms in Suppl. Fig. SI 2B), 3 additional *C1ql3* KO animals had unstable periods under LL conditions (third and fifth sets of actograms and periodograms in Suppl. Fig. SI 1, and third actogram and corresponding periodograms in Suppl. Fig. SI 2B), and 1 WT mouse had an unstable period in LL (third actogram and corresponding periodograms in Suppl. Fig. SI 2A). The arrhythmic mouse was excluded from phase angle, standard deviation of onsets, and period length measurements. All of the above-listed mice were excluded from period length measurements under LL conditions. Additionally, for beam break recordings, 1 *C1ql3* KO animal exhibited so much activity in the light portion of the 12:12 LD cycle that it was

not possible to accurately determine onsets of activity (last actogram and corresponding periodograms in Suppl. Fig. SI 3B). This animal was excluded from phase angle and standard deviation of onsets measurements.

RESULTS

C1ql3 Is Expressed in the SCN

To examine the expression pattern of *C1ql3*, we used mice harboring an allele *(C1ql3^{flox})* in which an essential exon is floxed and IRES-mVenus is knocked into the endogenous 3′ UTR of the *C1ql3* locus, such that mVenus marks all *C1ql3*-expressing cells (Martinelli et al., 2016). The mVenus is not tethered to the C1QL3 protein and thus will fill all neuronal compartments. The mVenus expression levels were low, so the signal was amplified by performing immunofluorescence for mVenus. We examined sagittal and coronal brain cryosections of adult *C1ql3$^{flox/flox}$* mice (Fig. 1, A–G). As described previously, mVenus/*C1ql3*-expressing neurons were prominent in multiple brain regions including the dentate gyrus (DG), the basolateral amygdala (BLA), and several cortical areas (Fig. 1A, 1F) (Martinelli et al., 2016). In addition, we observed expression of *C1ql3* in the paraventricular nucleus of the thalamus (PVT), in the SCN, and in fibers dorsal to the SCN, which may be arising from the reciprocal circuit between the PVT and the SCN (Fig. 1A, 1D, 1E) (Colavito et al., 2015; Moga and Moore, 1997; Moga et al., 1995; Vertes and Hoover, 2008). Moga and Moore (1997) described the PVT efferents to SCN as being present throughout the SCN with greater density in the dorsomedial area. A previous in situ hybridization analysis reported that *C1ql3* expression in the hypothalamus was specific to the arcuate nucleus (Iijima et al., 2010); however, we did not observe any mVenus-positive soma in this region. Using co-labeling of mVenus expression with immunofluorescence for vasoactive intestinal peptide (VIP), which is expressed in the SCN and not the arcuate nucleus, we clearly show that *C1ql3* is expressed in the SCN (Fig. 1, B–D) and not in the arcuate nucleus (Fig. 1F, 1G). In the telencephalon, *C1ql3* is expressed in excitatory neurons (Martinelli et al., 2016); however, most neurons of the SCN are GABAergic (Moore and Speh, 1993). Thus, it is very likely that *C1ql3* is expressed in GABAergic neurons in the SCN.

C1ql3 Expression Is Not Restricted to a Specific Population of SCN Neurons

Identifying which SCN cell types express *C1ql3* could provide clues as to its function. The SCN can be roughly divided into shell and core regions based on its neuronal projections and neuropeptide expression. An initial qualitative assessment suggested that *C1ql3* expression might be specific for neurons of the shell, as there appears to be less mVenus signal in the SCN core (Fig. 2, A–C). The SCN contains subsets of neurons that express specific neuropeptides, such as arginine vasopressin (AVP), gastrin-releasing peptide (GRP), and VIP (Abrahamson and Moore, 2001; Fernandez et al., 2016; Karatsoreos et al., 2004; Welsh et al., 2010). VIP neurons are found in the ventral portion of the SCN (Abrahamson and Moore, 2001), and we observed incomplete co-expression between VIP and *C1ql3*. Quantification of co-localized cells revealed that approximately 55% of VIP-positive cells also expressed *C1ql3* and approximately 8% *C1ql3*-positive cells also expressed VIP (Fig. 2A, 2H). Consistent with previous reports (Abrahamson and Moore, 2001), we observed AVP expression predominantly in neurons located in the dorsal/shell part of the SCN;

however, there was also incomplete co-expression between AVP and *C1ql3*. Approximately 28% of AVP-positive cells expressed *C1ql3* and approximately 11% of *C1ql3*-positive cells also expressed AVP (Fig. 2C, 2D, 2H). As expected, immunohistochemistry for GRP predominantly labeled projections rather than cell bodies (Drouyer et al., 2010); therefore, we could not discriminate the GRP-expressing neurons (Fig. 2B). We conclude that although there appears to be a topographic SCN organization for *C1ql3*-expressing cells, it is unclear what this organization is. Additionally, the expression pattern of *C1ql3* only partially overlaps with several neuropeptides, and the significance of this is not yet apparent.

Multiple neuropeptides are important for SCN function. We sought to determine whether loss of *C1ql3* has effects on neuropeptide expression in the SCN. We converted the $C1ql3^{flox}$ allele into a null allele $(C1ql3^{-})$ by using germline expression of Crerecombinase. Constitutive homozygous *C1ql3* KO mice $(C1ql3^{-/-})$ and wild-type littermate controls $(C1ql3^{+/+})$ were obtained by breeding heterozygous parents. As described by Martinelli et al. (2016), there is no detectable *C1ql3* expression in $C1ql3^{-/-}$ mice. We performed immunofluorescence for VIP, GRP, and AVP in control and *C1ql3* KO SCNs obtained from mice sacrificed at the same zeitgeber time. There did not appear to be any obvious change in VIP, GRP, or AVP immunoreactivity in the SCN from *C1ql3* KO mice (Fig. 2, E–G) compared with control SCN.

C1QL3 Regulates Excitatory Synaptic Density in the SCN

Given the function of C1QL3 in regulating synaptic density in the telencephalon, we sought to determine whether C1QL3 has a similar role in the SCN. We quantified immunofluorescent puncta density of synaptophysin (SYP), a general presynaptic marker, in the SCN in wild-type and *C1ql3* KO mice. We found reduced synapse density in *C1ql3* KO mice (Fig. 3A, 3B). To determine whether this reduction was due to a decrease in excitatory or inhibitory synapses (or both), we stained for VGluT2, a presynaptic marker for excitatory synapses, and VGAT, a presynaptic marker for inhibitory synapses (Fig. 3C, 3D). We observed a significant decrease in VGluT2-positive puncta in the SCN of *C1ql3* KO mice, whereas there was no significant change in VGAT-positive puncta.

These data suggest that, similar to its role in the telencephalon, C1QL3 is involved in regulating excitatory synaptic density in the SCN. This is despite the expression of C1QL3 in GABAergic neurons, suggesting there are important mechanistic differences depending on the cell type in which *C1ql3* is expressed. Perhaps C1QL3 protein is not released presynaptically as was observed from excitatory neurons (Martinelli et al., 2016; Matsuda et al., 2016) but is postsynaptic, or perhaps C1QL3 is secreted and diffusible and could thus function non-cell-autonomously. Alternatively, the reduced excitatory synapse density in the SCN observed in *C1ql3* KO mice could be due to a decrease in synapses from glutamatergic *C1ql3*-expressing neurons that project into the SCN. Most glutamatergic input to the SCN originates from the retina. To determine whether *C1ql3* is expressed in the retina, we examined retinas from $C1ql3^{flox/flox}$ mice and co-stained for mVenus and BRN3A, a marker for many retinal ganglion cells (RGCs). We found that *C1ql3* is expressed in a subset of RGCs (Fig. 4A). Only a small subset of RGCs project to the SCN and therefore could potentially contribute to the reduced excitatory synapse density observed in the SCN of

mutant mice. Intrinsically photosensitive RGCs (ipRGCs), which express the photopigment melanopsin, constitute the entire retinal projection to the SCN (Güler et al., 2008). When we co-stained for melanopsin and mVenus in retinas from *C1ql3*$^{flox/flox}$ mice, we observed no co-localization between *C1ql3*-positive RGCs and melanopsin-positive RGCs (Fig. 4B). Thus, while *C1ql3* is expressed by a subset of RGCs, it is not expressed in SCN projecting ipRGCs and loss of glutamatergic synapses in the SCN is not due to a loss of *C1ql3* expression from retinal afferents. Another source of glutamatergic input to the SCN is the PVT, which also expresses *C1ql3* (Fig. 1E) and has reciprocal connections with the SCN (Alamilla and Aguilar-Roblero, 2010; Colavito et al., 2015; Cui et al., 2001; Zhang et al., 2006). It is possible that the reduction in VGluT2-positive puncta in the SCN of *C1ql3* KO mice is due to a reduction in glutamatergic inputs from the PVT, although we have not tested this possibility here.

C1ql3 KO Mice Exhibit Period Lengthening following a 15-Minute Phase-delaying Light Pulse and Less Consolidated Activity

We sought to investigate effects of the observed altered synaptic circuit structure on circadian rhythms. We analyzed the wheel-running behavior of adult littermate wild-type and *C1ql3* KO mice in standard 12/12 LD, DD, and LL (representative actograms and chi-square periodograms are shown in Fig. 5A, additional actograms and periodograms in Suppl. Figs. SI 1–2). We generated chi-square periodograms for each of the LD, DD, and LL portions of the recordings (Fig. 5A, Suppl. Figs. SI 1–2). During LD conditions, we quantified the phase angle of photoentrainment and the standard deviation of the onset of activity during photoentrainment. By all of these measures, *C1ql3* KO mice displayed circadian photoentrainment that was similar to controls, although 1 *C1ql3* KO mouse was arrhythmic as determined by chi-square periodograms (Suppl. Fig. SI 2B). We also measured general home cage activity by recording infrared beam-breaks, and the periodograms as well as quantification of phase angle and standard deviation of the onset of activity (Suppl. Figs. SI 3, 4A, B) also supported the conclusion that *C1ql3* KO mice can photoentrain.

During recordings of general activity (beam breaks) we exposed the mice to a “jet-lag” paradigm (shift in the LD cycle) and varied the intensity of light during this paradigm. There was no difference in the rate of reentrainment between genotypes (Suppl. Figs. SI 3, 4C). We also assessed positive masking during reentrainment to the shifts in the LD cycle. Unsurprisingly, since masking is known to be independent of the SCN (Redlin and Mrosovsky, 1999), *C1ql3* KOs were comparable to WT mice (Suppl. Figs. SI 3, 4D).

While *C1ql3* KO mice clearly photoentrained under a 12/12 LD cycle, analysis of wheel-running activity revealed a phenotype with variable penetrance. We quantified total number of wheel revolutions that occurred in the light and dark portions of the 12/12 LD cycle, as well as the relative amount of activity that occurred in the dark portion. *C1ql3* KO animals exhibited increased activity in the light portion of the LD cycle compared with the WT controls. Specifically, from a total of 11 mutant mice, 5 displayed this less consolidated rhythm as indicated by increased activity during the light portions of the day (Fig. 5, A–C).

Less consolidated activity under LD conditions is suggestive of a disrupted, weakly oscillating, or less robust clock. In other mouse mutants that have a disrupted or weakly oscillating SCN clock due to loss of components of the transcriptional-translational feedback loop or of neuropeptides, behavioral rhythms further degenerate in the absence of light (Aton et al., 2005; Bae et al., 2001; Colwell et al., 2003; van der Horst et al., 1999; Vitaterna et al., 1999; Zheng et al., 2001). To determine whether this was also the case in *C1ql3* KO mice, we placed animals under constant dark conditions (DD). When *C1ql3* KO mice were placed under DD and allowed to "free-run," the phenotype did not worsen and their intrinsic period (tau) (measured by both periodograms and regression lines of the slope of the onsets of activity) was indistinguishable from that of controls (Fig. 5A, 1G, Suppl. Figs. SI 1–3). These data suggest that *C1ql3* KO mice do not have a disrupted or weakly oscillating circadian clock. This finding is also consistent with our observation that neuropeptide expression is not drastically altered in *C1ql3* KO mice.

Various light environments have been documented to induce circadian aftereffects. In addition to period shortening and lengthening after entrainment to short and long days, respectively, very small aftereffects can even be observed after a 15-minute phase shifting light pulse is given under DD (Pittendrigh and Daan, 1976). Phase-shifting pulses that result in phase delays cause period lengthening, and phase-shifting pulses that cause phase advances result in period shortening (Pittendrigh and Daan, 1976). To begin to investigate whether C1QL3 has any role in mediating aftereffects, we challenged *C1ql3* KO mice with mildly disruptive light exposure. Pittendrigh and Daan (1976) reported that a 15-minute light pulse under constant dark conditions results in mild and inconsistent, yet significant, aftereffects. When we exposed mice to a 15-minute light pulse at CT 15 in DD (asterisk in Fig. 5A), we were surprised to observe that the intrinsic circadian period of all *C1ql3* KO mice was substantially lengthened (Fig. 5A, 5G, 5H; Suppl. Figs. SI 1–3), while phase shifting was comparable to that of WT mice (Fig. 5F). While we did not do so here, it will be important in future work to determine the effects of phase-advancing light pulses.

According to Aschoff's rule, circadian period length increases with light intensity (Aschoff, 1960; Pittendrigh, 1960), and at very high light intensities mice become arrhythmic (Daan and Pittendrigh, 1976b). When wild-type and *C1ql3* KO mice were placed in LL, they exhibited comparable period lengths (Fig. 5I). However, 4 of 10 *C1ql3* KO mice and 1 WT mouse, as determined by the chi-square periodograms, appeared to be arrhythmic or had unstable periods under LL conditions (Suppl. Figs. SI 1, 2). These mice had to be excluded from the quantification of period length under LL. This effect could be due to the role of C1QL3 in consolidating activity. Alternatively, constant light is known to cause severe aftereffects that result in the lengthening of the intrinsic circadian period. Thus, the arrhythmia exhibited by several of the *C1ql3* KO mice after exposure to LL could be due to a combinatorial effect of the normal period lengthening that occurs under LL conditions and potential enhanced aftereffects due to loss of *C1ql3*.

DISCUSSION

Proper brain function is based on neuronal networks, which in turn are based on synapses, the fundamental structural unit by which neurons communicate. A multitude of proteins act

as crucial facilitators for neurons to connect via synapses into complex networks. Proteins of the C1q/tumor necrosis factor (TNF) superfamily have recently entered the spotlight for their function at synapses. Several members of this superfamily, including C1q, CBLN1, C1QL1, and C1QL3, have been shown to modulate synapse numbers (Kakegawa et al., 2015; Martinelli et al., 2016; Matsuda et al., 2010; Stevens et al., 2007). Although details for the molecular mechanisms are scant, it is likely that the C1QL family functions in a unique pathway compared with other superfamily members, as the surfaces of the proteins are largely unique (Ressl et al., 2015). C1QL3 is expressed in a small subset of brain regions, predominantly in the telencephalon. We recently demonstrated that C1QL3 is targeted presynaptically and functions to promote synapse maintenance and/or synaptogenesis in the telencephalon (Martinelli et al., 2016). Given that *C1ql3* appeared to be expressed only in excitatory projection neurons, we speculated that in each circuit where the gene was expressed, C1QL3 would have a function in promoting excitatory synapse density.

In this work, we made 3 principal observations. First, we discovered that *C1ql3* is expressed in the SCN of the hypothalamus, not the arcuate nucleus as was previously reported (Fig. 1). *C1ql3* is expressed in a subset of SCN neurons and more predominantly in the SCN shell, although it is not a marker for any specific neuron subtype that we have tested thus far (Fig. 2). Since the neurons of the SCN are predominantly GABAergic, this indicates that *C1ql3* expression cannot be excitatory-specific, as was thought previously. Second, the SCN of *C1ql3* KO mice have a reduced excitatory synapse density (Fig. 3), which parallels the reduced excitatory synapse density observed in KO telencephalon. This suggests that C1QL3 has a similar function at synapses although expressed in different brain regions. It is not immediately clear how it can do so, if the gene is expressed in the inhibitory neurons of the SCN. Third, *C1ql3* KO mice display altered circadian activity, including less consolidated activity to the dark portion of the LD cycle and period lengthening after a 15-minute light pulse in constant darkness, which could suggest a role for *C1ql3* in mediating the magnitude of aftereffects (Fig. 5, Suppl. Figs. SI 1–3).

How exactly can the supposedly presynaptically targeted C1QL3 influence excitatory synapse density in the SCN? We propose 3 possibilities. First, C1QL3 is expressed in the GABAergic neurons of the SCN but, rather than being released from the GABAergic presynaptic terminals, is located postsynaptically at the excitatory synapses of the C1QL3-expressing SCN neurons. Second, C1QL3 can act non-cell-autonomously at the excitatory synapses of SCN afferents. Our previous research in the telencephalon suggested a cell-autonomous function, but it is possible that C1QL3 protein is secreted and diffuses to nearby synapses of other neurons, regardless of how it is secreted. Third, while we show that C1QL3 is not expressed by retinal excitatory afferents, C1QL3 could be expressed in other excitatory neurons that send projections into the SCN, such as the PVT, and contribute to the excitatory synapses of these projections. It would need to be confirmed that there indeed exist *C1ql3*-expressing neurons within the PVT that project into the SCN. More investigation in this area will reveal whether the reduction in excitatory synapses in the SCN in *C1ql3* KO mice is due to a loss of intra-SCN connections or whether there is a reduction in SCN afferents, but this is beyond the scope of the present study.

C1QL3 has recently been shown to bind the kainate receptors GluK2 and GluK4 in the hippocampus and, through a complex with neurexin-3, specifically regulates recruitment of GluK2 and GluK4 to the postsynapse (Matsuda et al., 2016). GluK2 and neurexin-3 are both expressed in the SCN (Lein et al., 2007; van den Pol et al., 1994), although binding of C1QL3 to kainate receptors was not shown to change synapse density. The family members C1QL1 and C1QL3 both bind to the postsynaptic GPCR BAI3 with strong affinity, and the C1QL1-BAI3 interaction was shown to be important for synapse numbers in the cerebellum (Bolliger et al., 2011; Kakegawa et al., 2015; Sigoillot et al., 2015). It remains to be determined whether BAI3 is present in the SCN and what role it might have.

Aftereffects on the free-running period are caused by different photoperiods and by light pulse–induced phase shifts (Daan and Pittendrigh, 1976a). Aftereffects on period length provide a mechanism to improve entrainment by adjusting the free-running period to be closer to the period of the environmental light-dark cycle. Too large a difference between the free-running period and the environmental light-dark cycle could lead to a failure to entrain. In humans, the difference between the free-running period and the period of the environmental light-dark cycle may be associated with morning or evening preferences (Duffy et al., 2001) and may underlie advanced or delayed sleep phase disorders. C1QL3-dependent regulation of synaptic density in the SCN allowed us to investigate a possible physiological mechanism for the poorly understood phenomenon of circadian aftereffects. *C1ql3* KO mice, which have altered synaptic circuit structure in the SCN, exhibited period lengthening following a 15-minute light pulse in DD, which is suggestive of enhanced aftereffects. However, this is only a precursory insight into the elusive mechanism of circadian aftereffects. Additional behavior experiments will be needed, including examining the effects of phase-advancing light pulses as well as measuring aftereffects caused by T22 and T28 LD cycles. Thus, while future work is necessary to fully elucidate the mechanisms underlying aftereffects and the potential role of C1QL3 in aftereffects, the results presented here point to a possible role for the structure of synaptic circuits in effecting circadian aftereffects.

Supplementary Material

Refer to Web version on PubMed Central for supplementary material.

Acknowledgments

This paper was supported by grants from the NIH (MH052804 and MH086403 to T.C.S., R01-GM076430 to S.H.) and by fellowship from NIDA (F32 DA031654 to D.C.M.). We thank Seiji Nishino and Noriaki Sakai at the Stanford University Sleep and Circadian Neurobiology Laboratory for providing technical assistance regarding data analysis.

References

Abrahamson EE, Moore RY. Suprachiasmatic nucleus in the mouse: retinal innervation, intrinsic organization and efferent projections. Brain Res. 2001; 916:172–191. [PubMed: 11597605]

Alamilla J, Aguilar-Roblero R. Glutamate and GABA neurotransmission from the paraventricular thalamus to the suprachiasmatic nuclei in the rat. J Biol Rhythms. 2010; 25:28–36. [PubMed: 20075298]

Albrecht U, Oster H. The circadian clock and behavior. Behav Brain Res. 2001; 125:89–91. [PubMed: 11682098]

Aschoff J. Exogenous and endogenous components in circadian rhythms. Cold Spring Harb Symp Quant Biol. 1960; 25:11–28. [PubMed: 13684695]

Aschoff, J. Response curves in circadian periodicity. In: Aschoff, J., editor. Circadian Clocks. Amsterdam, The Netherlands: North-Holland; 1965. p. 95-111.

Aschoff, J. Handbook of Behavioral Neurobiology. New York: Plenum Press; 1981.

Aton SJ, Block GD, Tei H, Yamazaki S, Herzog ED. Plasticity of circadian behavior and the suprachiasmatic nucleus following exposure to non-24-hour light cycles. J Biol Rhythms. 2004; 19:198–207. [PubMed: 15155006]

Aton SJ, Colwell CS, Harmar AJ, Waschek J, Herzog ED. Vasoactive intestinal polypeptide mediates circadian rhythmicity and synchrony in mammalian clock neurons. Nat Neurosci. 2005; 8:476–483. [PubMed: 15750589]

Bae K, Jin X, Maywood ES, Hastings MH, Reppert SM, Weaver DR. Differential functions of mPer1, mPer2, and mPer3 in the SCN circadian clock. Neuron. 2001; 30:525–536. [PubMed: 11395012]

Balsalobre A, Damiola F, Schibler U. A serum shock induces circadian gene expression in mammalian tissue culture cells. Cell. 1998; 93:929–937. [PubMed: 9635423]

Barrett RK, Page TL. Effects of light on circadian pacemaker development, I: the freerunning period. J Comp Physiol A. 1989; 165:41–49. [PubMed: 2585358]

Bolliger MF, Martinelli DC, Sudhof TC. The cell-adhesion G protein-coupled receptor BAI3 is a high-affinity receptor for C1q-like proteins. Proc Natl Acad Sci U S A. 2011; 108:2534–2539. [PubMed: 21262840]

Colavito V, Tesoriero C, Wirtu AT, Grassi-Zucconi G, Bentivoglio M. Limbic thalamus and state-dependent behavior: the paraventricular nucleus of the thalamic midline as a node in circadian timing and sleep/wake-regulatory networks. Neurosci Biobehav Rev. 2015; 54:3–17. [PubMed: 25479103]

Colwell CS, Michel S, Itri J, Rodriguez W, Tam J, Lelievre V, Hu Z, Liu X, Waschek JA. Disrupted circadian rhythms in VIP- and PHI-deficient mice. Am J Physiol Regul Integr Comp Physiol. 2003; 285:R939–R949. [PubMed: 12855416]

Cui LN, Coderre E, Renaud LP. Glutamate and GABA mediate suprachiasmatic nucleus inputs to spinal-projecting paraventricular neurons. Am J Physiol Regul Integr Comp Physiol. 2001; 281:R1283–R1289. [PubMed: 11557637]

Daan S, Pittendrigh CS. Functional-analysis of circadian pacemakers in nocturnal rodents, 2: variability of phase response curves. J Comp Physiol. 1976a; 106:253–266.

Daan S, Pittendrigh CS. Functional-analysis of circadian pacemakers in nocturnal rodents, 3: heavy-water and constant light—homeostasis of frequency. J Comp Physiol. 1976b; 106:267–290.

Dibner C, Schibler U, Albrecht U. The mammalian circadian timing system: organization and coordination of central and peripheral clocks. Annu Rev Physiol. 2010; 72:517–549. [PubMed: 20148687]

Drouyer E, LeSauter J, Hernandez AL, Silver R. Specializations of gastrin-releasing peptide cells of the mouse suprachiasmatic nucleus. J Comp Neurol. 2010; 518:1249–1263. [PubMed: 20151358]

Duffy JF, Rimmer DW, Czeisler CA. Association of intrinsic circadian period with morningness-eveningness, usual wake time, and circadian phase. Behav Neurosci. 2001; 115:895–899. [PubMed: 11508728]

Eskin A. Properties of the Aplysia visual system: in vitro entrainment of the circadian rhythm and centrifugal regulation of the eye. Zeitschrift für vergleichende Physiologie. 1971; 74:353–371.

Fernandez DC, Chang YT, Hattar S, Chen SK. Architecture of retinal projections to the central circadian pacemaker. Proc Natl Acad Sci U S A. 2016; 113:6047–6052. [PubMed: 27162356]

Güler AD, Ecker JL, Lall GS, Haq S, Altimus CM, Liao H-W, Barnard AR, Cahill H, Badea TC, Zhao H, et al. Melanopsin cells are the principal conduits for rod-cone input to non-image-forming vision. Nature. 2008; 453:102–105. [PubMed: 18432195]

Hamann J, Aust G, Arac D, Engel FB, Formstone C, Fredriksson R, Hall RA, Harty BL, Kirchhoff C, Knapp B, et al. International Union of Basic and Clinical Pharmacology, XCIV: adhesion G protein-coupled receptors. Pharmacol Rev. 2015; 67:338–367. [PubMed: 25713288]

Iijima T, Miura E, Watanabe M, Yuzaki M. Distinct expression of C1q-like family mRNAs in mouse brain and biochemical characterization of their encoded proteins. Eur J Neurosci. 2010; 31:1606–1615. [PubMed: 20525073]

Johnson CH, Elliott JA, Foster R. Entrainment of circadian programs. Chronobiol Int. 2003; 20:741–774. [PubMed: 14535352]

Jud C, Schmutz I, Hampp G, Oster H, Albrecht U. A guideline for analyzing circadian wheel-running behavior in rodents under different lighting conditions. Biol Proced Online. 2005; 7:101–116. [PubMed: 16136228]

Kakegawa W, Mitakidis N, Miura E, Abe M, Matsuda K, Takeo YH, Kohda K, Motohashi J, Takahashi A, Nagao S, et al. Anterograde C1ql1 signaling is required in order to determine and maintain a single-winner climbing fiber in the mouse cerebellum. Neuron. 2015; 85:316–329. [PubMed: 25611509]

Karatsoreos IN, Yan L, LeSauter J, Silver R. Phenotype matters: identification of light-responsive cells in the mouse suprachiasmatic nucleus. J Neurosci. 2004; 24:68–75. [PubMed: 14715939]

Lein ES, Hawrylycz MJ, Ao N, Ayres M, Bensinger A, Bernard A, Boe AF, Boguski MS, Brockway KS, Byrnes EJ, et al. Genome-wide atlas of gene expression in the adult mouse brain. Nature. 2007; 445:168–176. [PubMed: 17151600]

Martinelli DC, Chew KS, Rohlmann A, Lum MY, Ressl S, Hattar S, Brunger AT, Missler M, Sudhof TC. Expression of C1ql3 in discrete neuronal populations controls efferent synapse numbers and diverse behaviors. Neuron. 2016; 91(5):1034–1051. [PubMed: 27478018]

Matsuda K, Budisantoso T, Mitakidis N, Sugaya Y, Miura E, Kakegawa W, Yamasaki M, Konno K, Uchigashima M, Abe M, et al. Transsynaptic modulation of kainate receptor functions by C1q-like proteins. Neuron. 2016; 90:752–767. [PubMed: 27133466]

Matsuda K, Miura E, Miyazaki T, Kakegawa W, Emi K, Narumi S, Fukazawa Y, Ito-Ishida A, Kondo T, Shigemoto R, et al. Cbln1 is a ligand for an orphan glutamate receptor delta2, a bidirectional synapse organizer. Science. 2010; 328:363–368. [PubMed: 20395510]

Matsumoto S, Basil J, Jetton AE, Lehman MN, Bittman EL. Regulation of the phase and period of circadian rhythms restored by suprachiasmatic transplants. J Biol Rhythms. 1996; 11:145–162. [PubMed: 8744242]

Meijer JH, Michel S, Vanderleest HT, Rohling JH. Daily and seasonal adaptation of the circadian clock requires plasticity of the SCN neuronal network. Eur J Neurosci. 2010; 32:2143–2151. [PubMed: 21143668]

Moga MM, Moore RY. Organization of neural inputs to the suprachiasmatic nucleus in the rat. J Comp Neurol. 1997; 389:508–534. [PubMed: 9414010]

Moga MM, Weis RP, Moore RY. Efferent projections of the paraventricular thalamic nucleus in the rat. J Comp Neurol. 1995; 359:221–238. [PubMed: 7499526]

Mohawk JA, Green CB, Takahashi JS. Central and peripheral circadian clocks in mammals. Annu Rev Neurosci. 2012; 35:445–462. [PubMed: 22483041]

Molyneux PC, Dahlgren MK, Harrington ME. Circadian entrainment aftereffects in suprachiasmatic nuclei and peripheral tissues in vitro. Brain Res. 2008; 1228:127–134. [PubMed: 18598681]

Moore RY, Speh JC. GABA is the principal neurotransmitter of the circadian system. Neurosci Lett. 1993; 150:112–116. [PubMed: 8097023]

Nagoshi E, Saini C, Bauer C, Laroche T, Naef F, Schibler U. Circadian gene expression in individual fibroblasts: cell-autonomous and self-sustained oscillators pass time to daughter cells. Cell. 2004; 119:693–705. [PubMed: 15550250]

O'Neill JS, Reddy AB. Circadian clocks in human red blood cells. Nature. 2011; 469:498–503. [PubMed: 21270888]

Pittendrigh CS. Circadian rhythms and the circadian organization of living systems. Cold Spring Harb Symp Quant Biol. 1960; 25:159–184. [PubMed: 13736116]

Pittendrigh CS, Daan S. Functional-analysis of circadian pacemakers in nocturnal rodents, 1: stability and lability of spontaneous frequency. J Comp Physiol. 1976; 106:223–252.

Redlin U, Mrosovsky N. Masking by light in hamsters with SCN lesions. J Comp Physiol A. 1999; 184:439–448. [PubMed: 10377978]

Refinetti, R. Circadian Physiology. 2nd. Boca Raton, FL: CRC Press; 2005.

Ressl S, Vu BK, Vivona S, Martinelli DC, Sudhof TC, Brunger AT. Structures of C1q-like proteins reveal unique features among the C1q/TNF superfamily. Structure. 2015; 23:688–699. [PubMed: 25752542]

Scheer FA, Wright KP Jr, Kronauer RE, Czeisler CA. Plasticity of the intrinsic period of the human circadian timing system. PLoS One. 2007; 2:e721. [PubMed: 17684566]

Sigoillot SM, Iyer K, Binda F, Gonzalez-Calvo I, Talleur M, Vodjdani G, Isope P, Selimi F. The secreted protein C1QL1 and its receptor BAI3 control the synaptic connectivity of excitatory inputs converging on cerebellar Purkinje cells. Cell Rep. 2015; 10(5):820–832.

Stevens B, Allen NJ, Vazquez LE, Howell GR, Christopherson KS, Nouri N, Micheva KD, Mehalow AK, Huberman AD, Stafford B, et al. The classical complement cascade mediates CNS synapse elimination. Cell. 2007; 131:1164–1178. [PubMed: 18083105]

van den Pol AN, Hermans-Borgmeyer I, Hofer M, Ghosh P, Heinemann S. Ionotropic glutamate-receptor gene expression in hypothalamus: localization of AMPA, kainate, and NMDA receptor RNA with in situ hybridization. J Comp Neurol. 1994; 343:428–444. [PubMed: 8027451]

van der Horst GT, Muijtjens M, Kobayashi K, Takano R, Kanno S, Takao M, de Wit J, Verkerk A, Eker AP, van Leenen D, et al. Mammalian Cry1 and Cry2 are essential for maintenance of circadian rhythms. Nature. 1999; 398:627–630. [PubMed: 10217146]

Vertes RP, Hoover WB. Projections of the paraventricular and paratenial nuclei of the dorsal midline thalamus in the rat. J Comp Neurol. 2008; 508:212–237. [PubMed: 18311787]

Vitaterna MH, Selby CP, Todo T, Niwa H, Thompson C, Fruechte EM, Hitomi K, Thresher RJ, Ishikawa T, Miyazaki J, et al. Differential regulation of mammalian period genes and circadian rhythmicity by cryptochromes 1 and 2. Proc Natl Acad Sci U S A. 1999; 96:12114–12119. [PubMed: 10518585]

Welsh DK, Takahashi JS, Kay SA. Suprachiasmatic nucleus: cell autonomy and network properties. Annu Rev Physiol. 2010; 72:551–577. [PubMed: 20148688]

Welsh DK, Yoo SH, Liu AC, Takahashi JS, Kay SA. Bioluminescence imaging of individual fibroblasts reveals persistent, independently phased circadian rhythms of clock gene expression. Curr Biol. 2004; 14:2289–2295. [PubMed: 15620658]

Yoo SH, Yamazaki S, Lowrey PL, Shimomura K, Ko CH, Buhr ED, Siepka SM, Hong HK, Oh WJ, Yoo OJ, et al. PERIOD2::LUCIFERASE real-time reporting of circadian dynamics reveals persistent circadian oscillations in mouse peripheral tissues. Proc Natl Acad Sci U S A. 2004; 101:5339–5346. [PubMed: 14963227]

Zhang L, Doroshenko P, Cao XY, Irfan N, Coderre E, Kolaj M, Renaud LP. Vasopressin induces depolarization and state-dependent firing patterns in rat thalamic paraventricular nucleus neurons in vitro. Am J Physiol Regul Integr Comp Physiol. 2006; 290:R1226–R1232. [PubMed: 16339383]

Zheng B, Albrecht U, Kaasik K, Sage M, Lu W, Vaishnav S, Li Q, Sun ZS, Eichele G, Bradley A, Lee CC. Nonredundant roles of the mPer1 and mPer2 genes in the mammalian circadian clock. Cell. 2001; 105:683–694. [PubMed: 11389837]

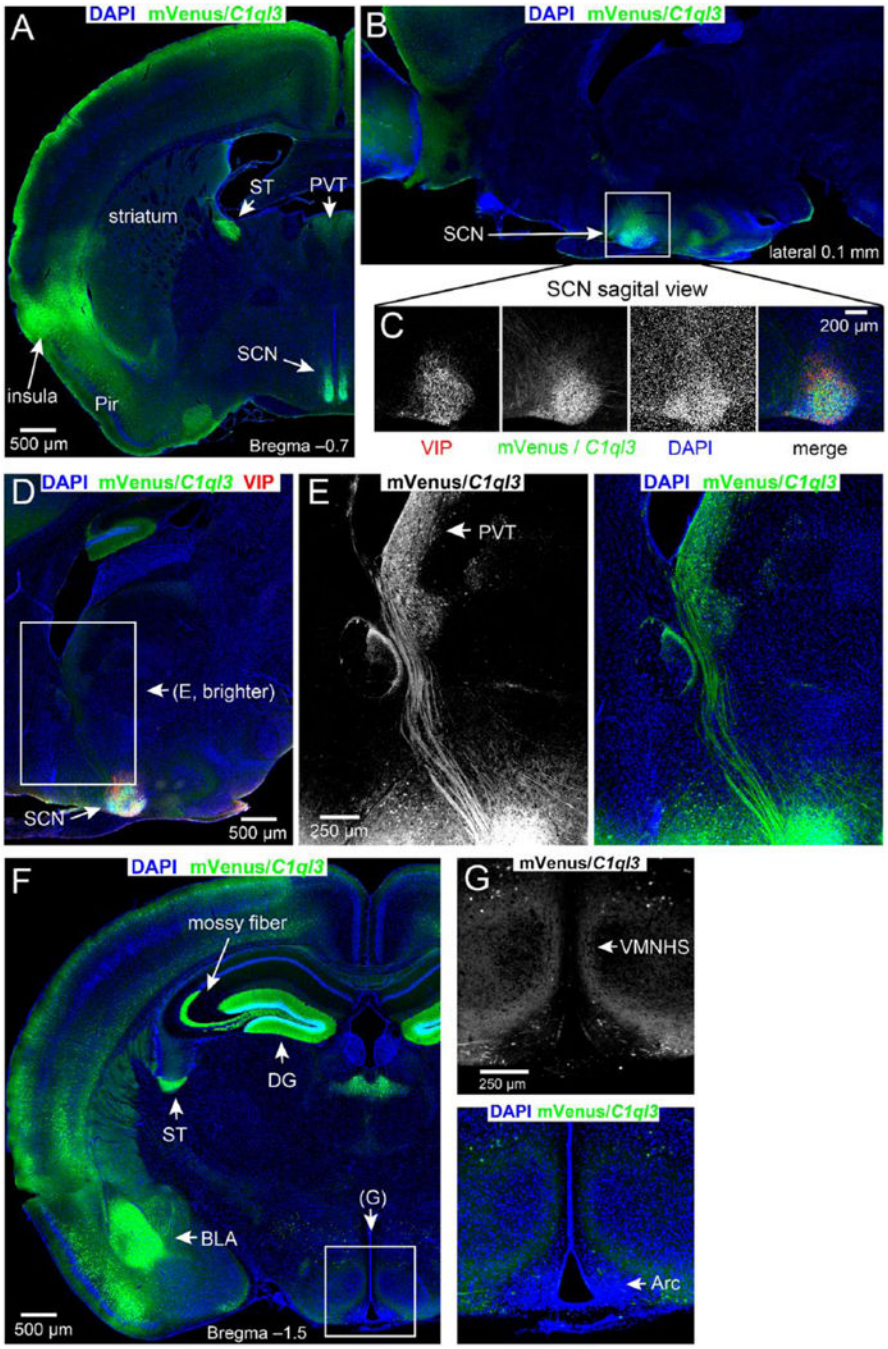

Figure 1.

C1ql3 is expressed in specific brain structures including the SCN and PVT. (A–G) Immunofluorescence staining of adult brain sagittal and coronal sections for mVenus in *C1ql3*-expressing cells and labeling with DAPI for cell nuclei. Arc, arcuate nucleus; DG, dentate gyrus; BLA, basolateral amygdala; Pir, piriform cortex; PVT, paraventricular nucleus of the thalamus; SCN, suprachiasmatic nucleus; ST, stria terminalis, VMNHS, ventromedial nucleus of the hypothalamus shell. (C) Magnification of the boxed region in Panel B. Also included is immunofluorescence for VIP, which is known to be expressed in

the SCN. (D) Identification of *C1ql3*-positive projections between the PVT and the SCN. (E) Magnification of boxed region in Panel D, and mVenus signal brightened to visualize axonal projections. (F) There is an absence of mVenus signal in the arcuate nucleus. (G) Magnification of the boxed region in Panel F. The arcuate nucleus lies ventral to the ventromedial nucleus.

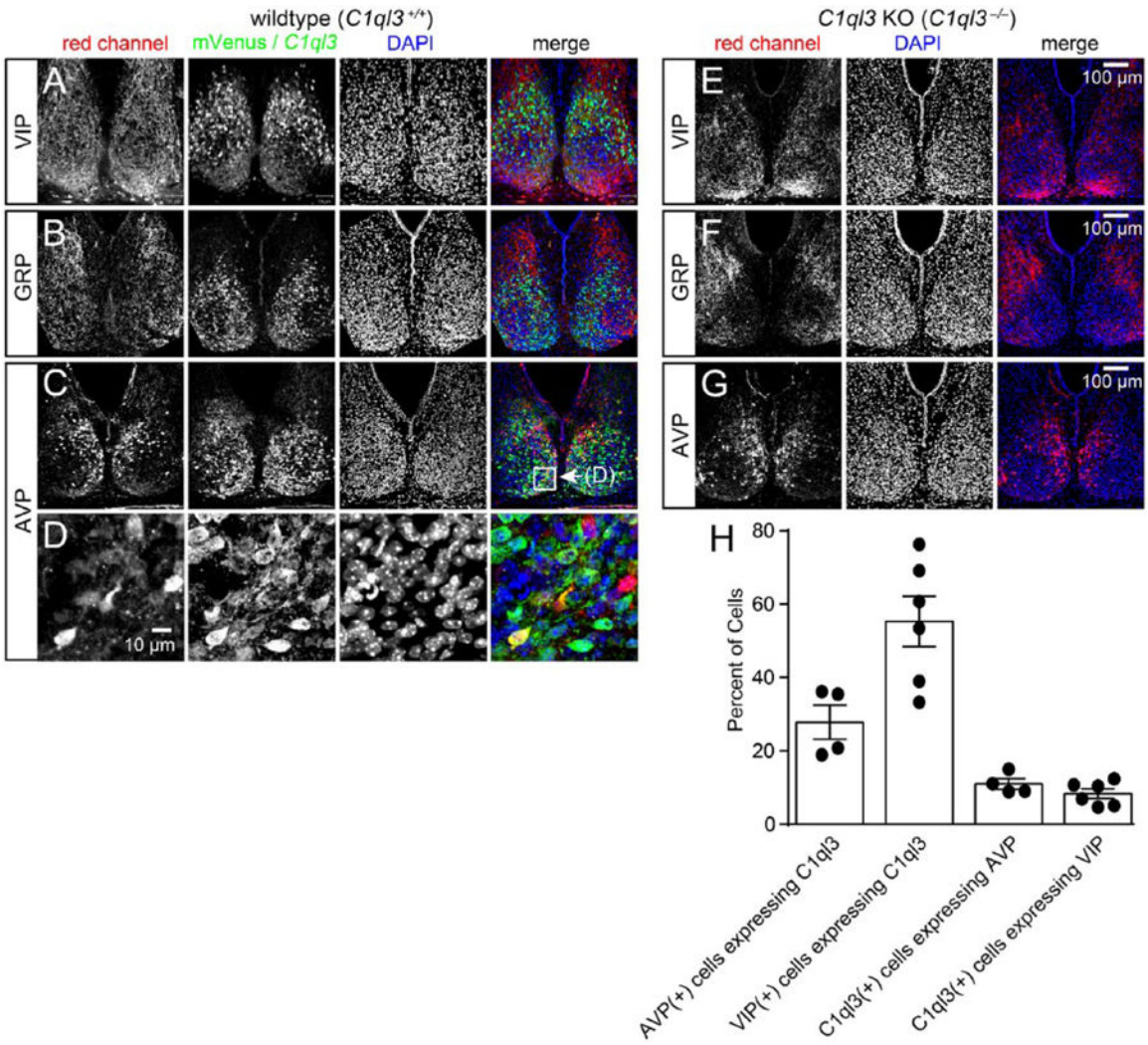

Figure 2.

C1ql3 is expressed in a subset of neurons in the SCN. (A–D) Representative immunofluorescence images for mVenus and neuronal markers in wild-type SCN. Panels A for VIP, Panels B for GRP, and Panels C for AVP. (D) Magnification of boxed region in Panel C. (E–G) Representative immunofluorescence images for VIP, GRP, and AVP, as indicated, in *C1ql3* KO SCN. Panels for mVenus expression were omitted as there was never any detectable mVenus expression in *C1ql3* KO mice. (H) Quantification of the percentage of AVP- and VIP-positive cells that co-express *C1ql3* as well as the percentage of *C1ql3*-positive cells that co-express either AVP or VIP. $n = 4$ brains stained for AVP, and $n = 6$ brains stained for VIP.

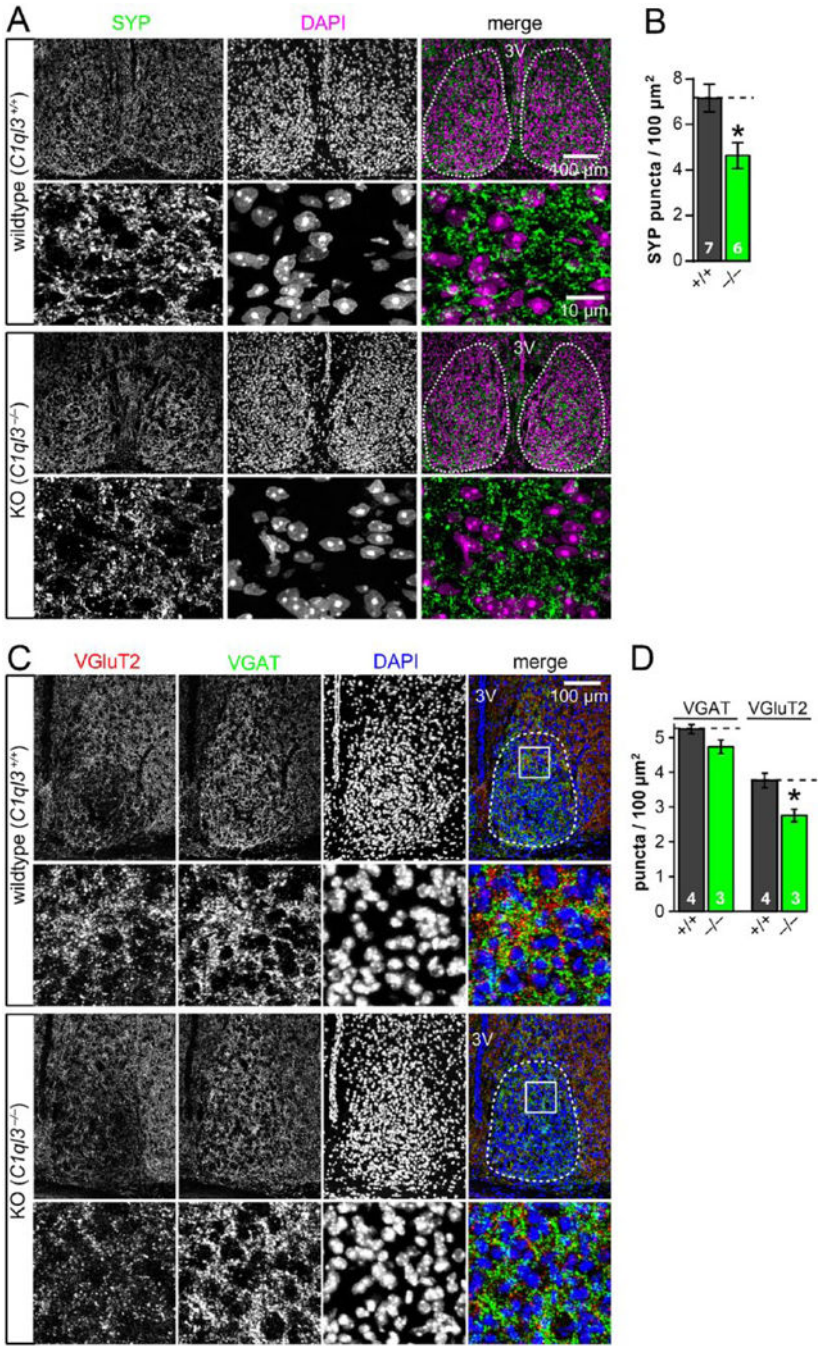

Figure 3.

C1QL3 regulates excitatory synapse density in the SCN. (A) *C1ql3* KO SCN had a decreased synapse density. Representative immunofluorescence images of SCN cryosections stained for synaptophysin (SYP) and DAPI. For each genotype, the upper image represents an overview of the SCN (dashed line = quantified area; 3V, third ventricle), and the lower image shows a representative high-magnification view. See Methods section for details on puncta quantification. Note that the high-magnification views were taken from a separate animal as from the overview image. (B) Summary graph of the density of synaptophysin-

positive synaptic puncta. WT (n = 7 brains) and KO (n = 6 brains). (C) *C1ql3* KO SCN had a decreased VGluT2-positive synapse density but not VGAT-positive synapse density. Representative immunofluorescence images of SCN cryosections stained for VGluT2, VGAT, and DAPI. For each genotype, the upper image represents an overview of the SCN (dashed line = quantified area; 3V, third ventricle), and the lower image shows a high-magnification view of the boxed region. (D) Summary graph of the density of VGluT2- and VGAT-positive synaptic puncta. WT (n = 4 brains) and KO (n = 3 brains). Data are means ± SEM; the number of mice analyzed is displayed in the graph. Statistical analyses were performed using 2-tailed t test. (*$p \leq 0.05$). See Supplementary Table SI 1. Refer to methods section for additional details on synaptic puncta quantification.

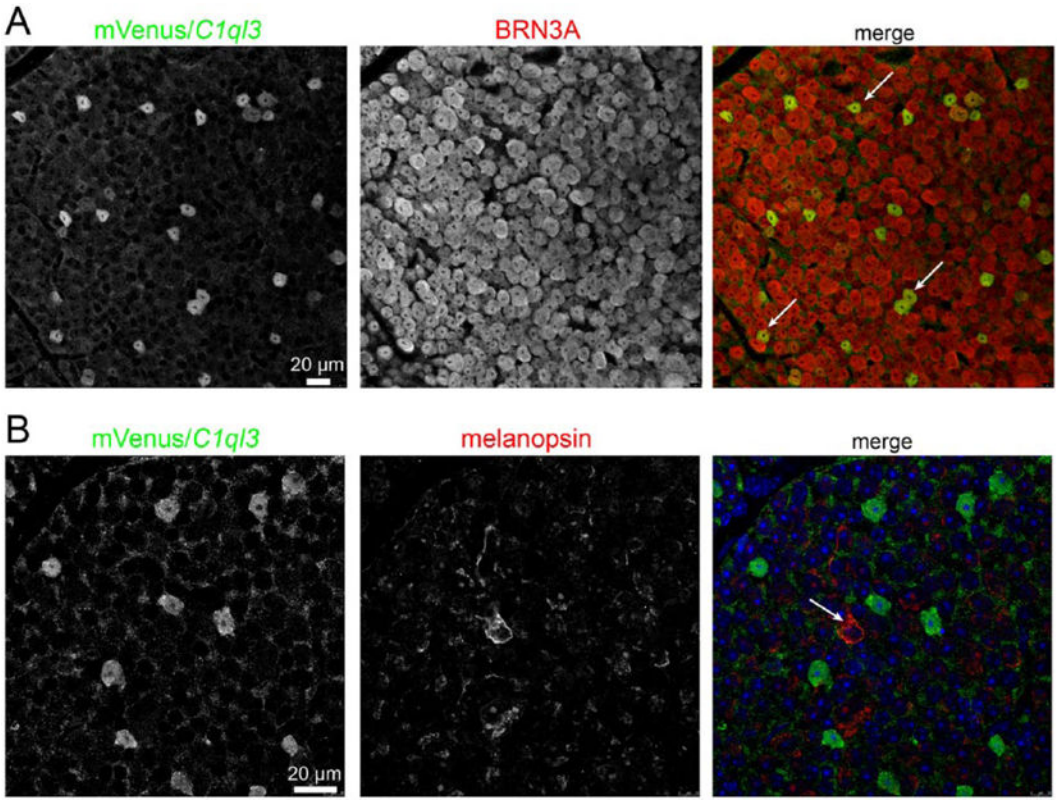

Figure 4.

C1ql3 expression in subset of RGCs. (A) Whole mounted retina from a *C1ql3*$^{flox/flox}$ mouse showing co-immunofluorescence for mVenus (green) and BRN3A (red), a marker for many RGCs. White arrows indicate co-localized cell bodies. (B) Whole mounted retina from a *C1ql3*$^{flox/flox}$ mouse showing co-immunofluorescence for mVenus (green) and melanopsin (red), a marker for ipRGCs, which project to the SCN. White arrows indicate the non-co-localized cell.

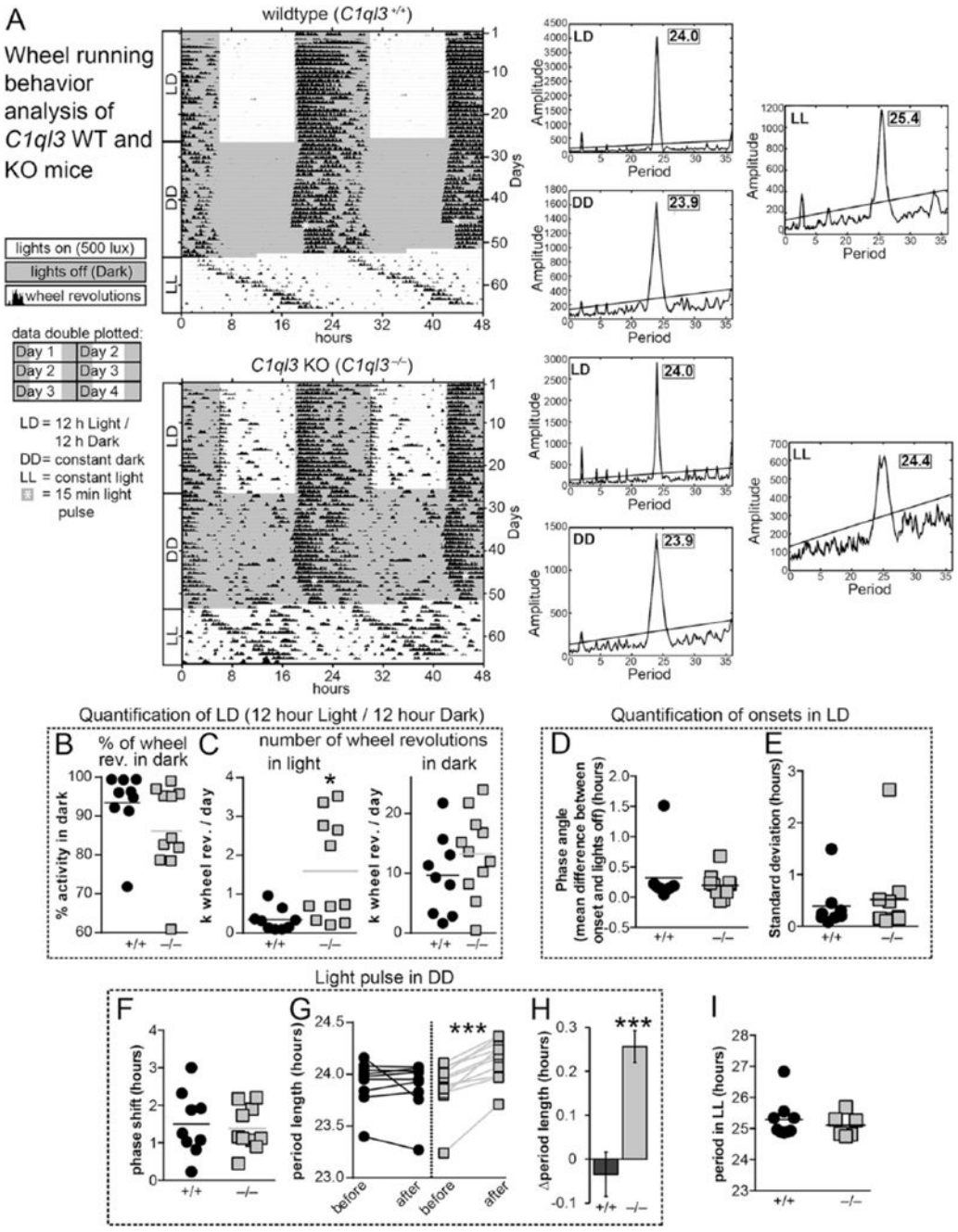

Figure 5.

C1ql3 KO mice exhibit behavioral abnormalities. (A) Representative wheel-running actograms for wild-type and *C1ql3* KO mice. Wheel revolutions are indicated by black markings in 10-min bins. Per convention, activity is double-plotted: 48 h per row, each 24-h day presented first on the right and again on the left on the subsequent row. Gray background denotes when lights were off; asterisk demarks a 15-min light pulse given in constant darkness. Chi-square periodograms were generated from portions of the recordings obtained while the mice were under LD, DD, and LL light conditions. (B) Wheel revolutions during standard 12:12 LD conditions, graphed as percentage of activity in the active phase.

Data points represent individual subjects, and horizontal lines the means. WT ($n = 9$) and KO ($n = 11$). (C) Total wheel revolutions in the light and dark portions of the day while housed in LD. WT ($n = 9$) and KO ($n = 11$). (D) Phase angle of photoentrainment during a 12:12 LD cycle. WT ($n = 8$) and KO ($n = 10$). (E) Mean standard deviation of the onset of activity during 12:12 LD cycle. WT ($n = 8$) and KO ($n = 10$). (F) Quantification of phase shifting caused by a 15-min light pulse administered at CT 15. Since *C1ql3* KO mice exhibited a change in period length following this light pulse, this measurement is based on the change in activity onset on the first day following the light pulse. WT ($n = 9$) and KO ($n = 10$). (G) Period length (tau) before and after a 15-min light pulse in DD, at CT 15. WT ($n = 9$) and KO ($n = 11$). (H) Quantification of the magnitude of the change in period length following the 15-min light pulse at CT 15. WT ($n = 9$) and KO ($n = 11$). (I) Period length under constant light conditions. WT ($n = 7$) and KO ($n = 6$). Statistical analyses were performed using 2-tailed *t* test for panels A-F, H, and I, and 2-way ANOVA with Bonferroni's multiple comparisons test for panel G (*$p \leq 0.05$, ***$p \leq 0.001$). See Suppl. Table SI 1.